

SDVRF: Sparse-to-Dense Voxel Region Fusion for Multi-modal 3D Object Detection

Binglu Ren

School of Artificial Intelligence
Beijing University of Posts and Telecommunications
Beijing, China
rbl@bupt.edu.cn

Jianqin Yin*

School of Artificial Intelligence
Beijing University of Posts and Telecommunications
Beijing, China
jqyin@bupt.edu.cn
* Corresponding author

Abstract—In the perception task of autonomous driving, multi-modal methods have become a trend due to the complementary characteristics of LiDAR point clouds and image data. However, the performance of previous methods is usually limited by the sparsity of the point cloud or the noise problem caused by the misalignment between LiDAR and the camera. To solve these two problems, we present a new concept, Voxel Region (VR), which is obtained by projecting the sparse local point clouds in each voxel dynamically. And we propose a novel fusion method, named Sparse-to-Dense Voxel Region Fusion (SDVRF). Specifically, more pixels of the image feature map inside the VR are gathered to supplement the voxel feature extracted from sparse points and achieve denser fusion. Meanwhile, different from prior methods, which project the size-fixed grids, our strategy of generating dynamic regions achieves better alignment and avoids introducing too much background noise. Furthermore, we propose a multi-scale fusion framework to extract more contextual information and capture the features of objects of different sizes. Experiments on the KITTI dataset show that our method improves the performance of different baselines, especially on classes of small size, including Pedestrian and Cyclist.

Index Terms—multi-modal, autonomous driving

I. INTRODUCTION

3D object detection aims to predict objects' locations, sizes, and classes in the 3D space with sensory input, which is a fundamental and crucial task in an automotive perception system. Reliable observations of objects around the ego vehicle will facilitate downstream components like trajectory prediction and path planning to enhance road safety [1, 2]. Among the numerous onboard sensors, LiDAR has great penetrability and provides accurate geometric information. Moreover, the camera provides rich semantic information for detection.

To leverage the complementary characteristics of different sensors, researchers have paid more and more attention to multi-modal 3D object detection in recent years, especially LiDAR-camera fusion methods. However, because of the physical limitations of LiDAR, points become extremely sparse when objects are far from the ego or occluded. Unlike point clouds, images can provide dense pixels even when objects are far apart. But it is hard to get high-accuracy 3D bounding boxes because lack of depth information in images.

The existing fusion strategies of associating sparse points with one or a few pixels still face the sparsity problem. Especially the detection accuracy of small classes, e.g., Pedestrian

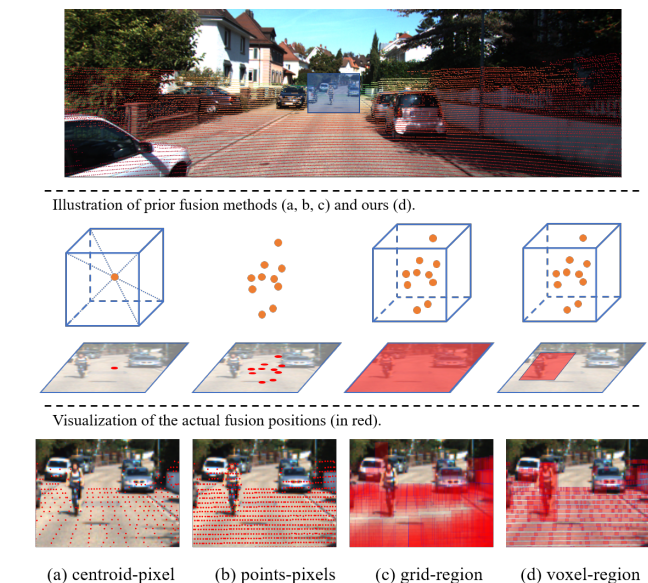


Fig. 1. **Top**: an image with point cloud projected. **Middle**: illustration of different fusion strategies, where the blue cubes are voxel grids, the orange points are point clouds, and the red areas are gathered pixels on the image plane. **Bottom**: visualization of the corresponding fusion strategies. (a): Fusion by projecting the voxel centroid and interpolation, which only samples a few pixels and is prone to misalignment. (b): Fusion in a point-to-pixel manner. The sampled pixels are still sparse, especially for small objects. (c): Fusion by projecting the evenly spaced voxel grids, which causes misalignment between modalities and introduces too much background noise. The darker red color indicates more overlaps between regions. (d): The voxel-region fusion we proposed to establish dense correspondence between a voxel and the image region while reducing background noise. The lighter red color indicates fewer overlaps and less noise.

and Cyclist, need to be improved. Most of these methods can be classified according to the granularity of fusion [3]. Point-level methods [4–11] usually use PointNet [12] to process the point clouds but fuse by establishing one-to-one indices between points and pixels, illustrated in Fig. 1 (b). RoI-level methods [13–16] usually fuse RoI features based on 2D or 3D proposals. Though the fusion granularity is denser, the performance of the whole model is likely to be limited by a single branch. The Voxel-level [17–20] granularity is finer than RoI-level. However, these methods have the problem of misalignment, which means the image pixels are likely to

be associated with wrong voxels, leading to more noise. As illustrated in Fig. 1 (c), the darker red area indicates more overlaps.

Focusing on developing a dense and effective fusion strategy, we propose a novel Sparse-to-Dense Voxel Region Fusion (SDVRF) method to boost the representation ability of fused features with rich contextual information, as shown in Fig. 1 (d). Concretely, the points are first divided evenly in space without downsampling operation [21]. Then we use points in every voxel to obtain a shape-variable rectangular area, named Voxel Region (VR), based on the calibration matrix of LiDAR and the camera. Notably, different from previous methods, which project the size-fixed voxels, the proposed VR is obtained flexibly according to the distribution of local point clouds. We also propose a multi-scale fusion framework to extract more contextual information and deal with objects of various sizes. We summarize our approach with two contributions:

Voxel Region Fusion Module. We proposed a new module to aggregate features from LiDAR point cloud and image by establishing dense correspondences between sparse points and dense pixels. Points in a voxel are considered a local point cloud, occupying a region in 3D space. We calculate an appropriate bounding box, i.e., the VR, for projected points on the image plane. The deep features of different modalities are fused within the region. Instead of attaching image features to points by sampling, or projecting the size-fixed grids, we gather more spatial context for the local point cloud while avoiding introducing too much noise. We also use a pre-trained semantic segmentation backbone to obtain image feature maps, reducing noise from images and accelerating convergence.

Multi-scale Voxelization Fusion Framework. Voxel-based methods usually face the problem of choice of voxel size. Previous LiDAR-based method voxelizes the point cloud by different sizes [22]. We further integrate local point clouds with image regions in various scales based on the proposed VRFM. Our network can generate the Bird’s-Eye View (BEV) features with rich geometric and contextual information.

II. RELATED WORK

A. 3D Object Detection Using LiDAR point clouds

LiDAR-based 3D object detection aims to predict target objects’ class, location, and direction from point clouds. LiDAR point clouds are irregular data with sparse distribution, and the number of points varies depending on the sample. Thus, special feature extraction methods are needed to make them processable by deep-learning models. Most methods can be classified into three categories. Point-based methods [23–30] adapt down-sampling to unify the number of points and ball query operation [12] to gather local features. These methods have a relatively flexible receptive field but may suffer information loss during sampling. Voxel-based methods first divide the point cloud into evenly sized grids and then extract features within each voxel. PointPillars [31] only voxelizes on BEV, thus can reduce computation. Voxel R-CNN [32] is proposed recently to refine detection based on coarse voxel

features. These methods have higher computational efficiency, but the ability of local feature extraction is limited by pre-defined voxel size. Point-voxel-based methods try to combine their strengths. HVNet [22] is proposed to fuse multi-scale voxel feature and point feature at point-level. PV-RCNN combines 3D voxel Convolutional Neural Network (CNN) with PointNet-based set abstraction operations [12].

B. LiDAR-camera fusion for 3D Object Detection

There is a huge modal gap between LiDAR point cloud and image data. A point cloud consists of sparsely irregularly distributed 3D coordinate data, while an image is a compact combination of pixels. LiDAR-camera-based methods usually focus on researching better fusion strategies. Fusion can be performed at different granularity [3]. Most methods can be classified into RoI-, point-, and voxel-wise. Specifically, RoI-wise methods usually depend on a single modal branch because fusion happens between 2D or 3D proposals. Point-wise fusion is more commonly used. MVX-Net [4] projects each point onto the image plane and appends the point with the image feature corresponding to the projected location index. PointPainting [6] is proposed to attach image segmentation scores onto points before they are fed into the network. EPNet [5] uses many Set Abstraction (SA) layers to extract key points features and fuse them with interpolated image features. These methods fuse in a point-to-pixel manner, which is a sparse correspondence. As for voxel-wise methods, MVX-Net [4] projects equally spaced grids before voxelization. DVF [33] samples image feature with projected voxel centers. These methods are either prone to introducing background noise or easily affected by alignment quality.

III. PROPOSED METHOD

A. Framework Overview

The overall architecture of the proposed SDVRF is illustrated in Fig. 2. First, the LiDAR point cloud and the matched monocular camera image are processed by separate streams. Multi-scale voxelization operation is applied to all the points and assigns every point to predefined voxels of different scales. The image is fed into a pre-trained image segmentation backbone to generate a semantic feature map. Then we gather and fuse them using VRFM within different scales. The VRFM can generate multi-modal features by establishing dense and appropriate correspondences for every occupied non-empty voxel. Further, features from different modalities are concatenated and scattered to BEV to recover a dense BEV feature map, then processed by a commonly used 3D detector, which is usually composed of a BEV backbone and a detection head. In the following, we present the technical details of the proposed method.

B. Image and LiDAR pipeline

Pixels are densely arranged in an image, and their rich semantic information can be gathered by convolution operations. However, LiDAR point clouds are sparse, irregularly distributed, and have highly variable point densities. Before

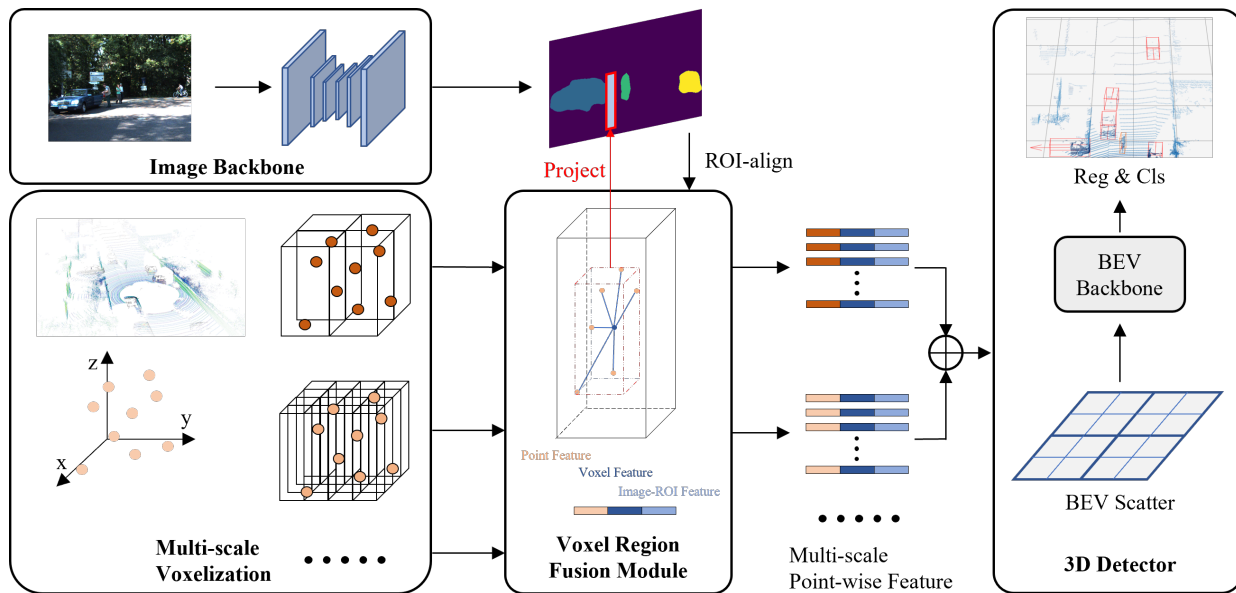


Fig. 2. Framework Overview. Each image is processed by a pre-trained semantic segmentation backbone to generate a feature map. The point cloud is voxelized with various scales and fed into the Voxel Region Fusion Modules (VRFMs, details in Section III-C) respectively. The points within each voxel are projected to obtain a region on the image plane dynamically. The multi-modal and multi-scale features are fused in the point level first and then converted to the voxel level (Section III-D). Finally, the boosted voxel features are fed into various 3D detectors to predict the final results.

feeding them into the proposed VRFM, we apply different pipelines as illustrated in Fig. 2.

For images captured by a monocular camera, we train a semantic segmentation backbone, i.e., LR-ASPP [34], to generate image feature maps $\mathbf{F}_{img} \in \mathbb{R}^{H \times W \times C}$. Each channel in the image feature map represents the confidence score for a specific category, including background. Notice that the parameters of these layers are frozen during training. For LiDAR point clouds, voxelization can divide points into an evenly spaced grid of voxels. The size of a voxel is predefined as (l, w, h) , representing length along X, Y, Z axes in 3D space. Following MVF [35], we use dynamic voxelization, which establishes the bi-directional mapping between points and voxels without sampling operation. For Multi-scale Voxelization Fusion Framework, we define different voxel sizes and apply voxelization within every scale. Point \mathbf{p}_i is assigned to voxels $\{\mathbf{v}_{j_0}, \dots, \mathbf{v}_{j_s}\}$ based on their relative spatial coordinates in different scales.

C. Voxel Region Fusion Module

Previous voxel-based fusion methods usually project the voxel centroids [16, 33] or the size-fixed grids [4] to sample the image feature. The former leads to sparse points fused with sparse pixels, while the latter introduces too much background noise. We further propose the VRFM to achieve a balance between generating dense fusion and introducing noise.

Projection from 3D to 2D. The VRFM takes all the points of a point cloud in field of view $\mathbf{P} = \{\mathbf{p}_1, \dots, \mathbf{p}_N\}$, their corresponding voxel indexes $\mathbf{I} = \{\mathbf{i}_1, \dots, \mathbf{i}_N\}$ in a single scale, and the image feature map \mathbf{F}_I as input. We use the transformation matrix \mathbf{M}_{tran} between LiDAR and

the camera and the camera’s intrinsic matrix \mathbf{M}_{intr} to project 3D points in world coordinate to image pixel coordinate. The transformation is expressed as

$$\mathbf{P}_{pix} = \mathbf{M}_{intr} \times \mathbf{M}_{tran} \times \mathbf{P} \div \mathbf{Z}_c \quad (1)$$

where \mathbf{P}_{pix} are homogeneous points in the pixel coordinates and \mathbf{Z}_c is the depth of points in the camera coordinate.

The above equations establish correspondences between the point cloud and the pixels. However, this projection heavily depends on the quality of the camera calibration matrices, including \mathbf{M}_{intr} and \mathbf{M}_{tran} . Small deviations can directly cause projection misalignment causing 3D points to be assigned to the wrong pixels. Some methods [16, 33] project the centroid of each voxel and assign one or a few pixels to the voxel, which is more likely to cause misalignment issues. Other methods [4] compute eight corners of each voxel and get a 2D ROI on the image. The projection of evenly spaced grids is effective but introduces too much background noise.

Generation of the Voxel Region. Based on the projection process above, we present the generation of VR. A local point cloud usually occupies a sub-space of the whole voxel space, defined as a 3D region. After projection, we get the 2D points \mathbf{P}_{pix} with one-to-one correspondence with the voxel indexes \mathbf{I} . The points within the same voxel share the same index. The number of points within each voxel and their location in local space varies.

With the help of the scatter max and min operations, we dynamically generate rectangle regions on the image plane for each voxel. The 2D region is defined by two corners $(x_{min}, y_{min}, x_{max}, y_{max})$, i.e., the axis-aligned minimum bounding box of the 2D points set. All the projected points of

the local point cloud are located in this 2D region. This can be formularized as follows:

$$\mathbf{R}_j = \text{Min}_i \{(x_i, y_i) \mid I_i = j\} \oplus \text{Max}_i \{(x_i, y_i) \mid I_i = j\} \quad (2)$$

where \mathbf{R}_j is the generated 2D region of voxel \mathbf{V}_j , and \oplus denotes concatenation operation.

To obtain more contextual information for voxels, we take the distance to the ego of 3D points into consideration. Points far away from the LiDAR are more sparse, which causes the number of points within a single voxel is too small. This may lead to failure to generate the 2D region under special circumstances, e.g., only one point in a voxel. We use a scaling factor to enlarge the width and length to generate 2D regions with appropriate areas. The range of the point clouds is defined as $[x_{min}, y_{min}, z_{min}, x_{max}, y_{max}, z_{max}]$, and the ego is at the origin of the LiDAR coordinate system. We compute the scale factor for the voxel \mathbf{V}_j as

$$\alpha_j = 1 + \frac{\| (x_j, y_j) \|}{\| (x_{max}, y_{max}) \|} \quad (3)$$

where (x_j, y_j) is the centroid of the voxel \mathbf{V}_j in BEV. The width w_j and length l_j of the Voxel Region are enlarged by multiplying the scale factor as

$$\begin{cases} w_j = \alpha_j (w_j + \delta) \\ l_j = \alpha_j (l_j + \delta) \end{cases} \quad (4)$$

where δ is the pre-defined offset to enlarge the region with zero area.

Extraction of the VR features. After the generation of the 2D region $\{R_j, j \in \mathbf{I}\}$, we extract features from different modalities, illustrated in Fig. 3. Following [31], the point features are encoded as $\mathbf{F}_P = P \oplus P_c$, shaped $N \times C_p$, where P_c is the relative coordinates with the centroids of voxels as the origin. The voxel features $\mathbf{F}_V \in \mathbb{R}^{V \times C_v}$ are extracted from point features by a simplified version of PointNet [12], which includes a linear layer followed by Batch-Norm, ReLU, and a max-pooling operation. The image voxel features $\mathbf{F}_I \in \mathbb{R}^{V \times C_i}$ are extracted from the image feature map using the voxel region. Specifically, the image voxel feature of the voxel \mathbf{V}_j is sampled by the RoI-align operation to create an output tensor of fixed size, i.e., a tensor shaped $C_i \times 7 \times 7$. Then the feature is flattened and reduced along channels by a linear layer followed by Batch-Norm and ReLU. This process is formulated as

$$\mathbf{F}_I^j = \text{MLP}(\text{Flat}(\text{Pool}(\mathbf{F}_{img}, \mathbf{R}_j))) \quad (5)$$

Then we fuse the features at point level by concatenation:

$$\mathbf{F}_{fuse} = \mathbf{F}_P \oplus M(\mathbf{F}_V) \oplus M(\mathbf{F}_I) \quad (6)$$

where M denotes the mapping operation from voxels to points using indexes \mathbf{I} .

The points obtained by LiDAR scanning are discrete and sparse. General voxel-level fusion methods [16, 33], which project the centroids of voxels (in Fig. 1 (a)), face the problem of sparsity. Moreover, other methods [4] project the equally

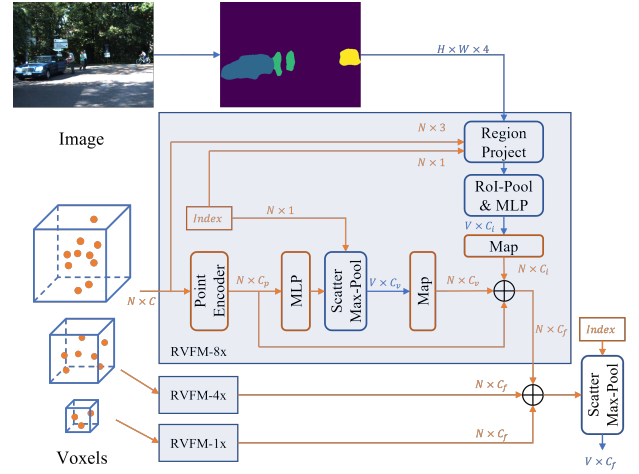


Fig. 3. Structure of the VRFM and the Multi-scale Voxelization Fusion Framework. Points within each voxel are encoded to voxel-level (blue) features by a PointNet-based module, including MLP and max-pooling. The points' coordinates and their indexes of voxels are fed into the Region Project module to generate corresponding regions and pooled into voxel-level image features. Afterward, these features are mapped back to point-level (orange) and fused by concatenation. At last, the fusion features from various scales are concatenated and pooled to the voxel level.

spaced grids introduce too much background noise, especially when points in a voxel are few or gather in a corner (in Fig. 1 (c), the red area is darker).

By establishing a dense mapping between a local point cloud and a dense image region, VRFM can gather contextual information within the appropriate range while avoiding introducing too much background noise. Dynamically generated regions have little overlap with each other (in Fig. 1 (d), the red area is lighter). Thus the problem of feature blurring [6] is alleviated. Moreover, VRFM is less sensitive to projection misalignment. When points of targets are projected to the background on the image caused by deviation, general sampling strategies may extract incorrect features. Still, VRFM is able to obtain correct regional features based on contextual information.

D. Multi-scale Voxelization Fusion Framework

The PointNet-based encoder used in most voxel-based methods operates on the unordered local point cloud and computes a unified feature vector by max-pooling. Thus, its ability to aggregate the local geometric and semantic information is associated with the space size of the voxel. Motivated by recent works [26, 33], which obtain multi-scale features by 3D convolution, we further proposed a Multi-scale Voxelization Fusion Framework based on the VRFM.

Voxelization divides the point clouds into evenly spaced grids, and the number of voxels is determined directly by the size of each voxel. Following HVNet [22], which encodes voxel information from different scales into the point-wise feature, we fuse multi-modal features in various voxel scales with the help of VRFM.

TABLE I
3D DETECTION RESULTS ON THE KITTI VAL SET USING $AP|_{R40}$ METRIC FOR MULTI-CLASS. THE MAP-S REFERS TO RESULTS ON SMALL OBJECTS. BEST IN BLUE, AND THE SECOND BEST IN GREEN. *DENOTES RE-PRODUCED RESULTS.

Modality	Methods	Reference	Car(%)				Pedestrian(%)				Cyclist(%)				mAP-S(%)	mAP(%)
			Easy	Mod.	Hard	mAP	Easy	Mod.	Hard	mAP	Easy	Mod.	Hard	mAP		
L	PointPillars* [31]	CVPR2019	86.83	78.09	75.44	80.12	57.44	51.95	47.14	52.18	80.28	63.07	58.71	67.35	59.77	66.55
	PointRCNN* [25]	CVPR2020	91.67	80.56	78.08	83.44	62.66	54.70	48.07	55.14	91.77	72.79	68.36	77.64	66.39	72.07
	PV-RCNN* [26]	CVPR2020	92.10	84.36	82.48	86.31	64.26	56.67	51.91	57.61	88.88	71.95	66.78	75.87	66.74	73.27
	Voxel R-CNN* [32]	AAAI2021	89.68	81.05	78.84	83.19	68.11	62.26	57.09	62.49	90.17	72.14	67.76	76.69	69.59	74.12
	FocalsConv [36]	CVPR2022	92.32	85.19	82.62	86.71	-	-	-	-	-	-	-	-	-	-
	PDV [37]	CVPR2022	92.56	85.29	83.05	86.97	66.90	60.80	55.85	61.18	92.72	74.23	69.60	78.85	70.02	75.67
L+I	3D-CVF [16]	ECCV2020	89.67	79.88	78.47	82.67	-	-	-	-	-	-	-	-	-	-
	PointPainting [6]	CVPR2020	88.38	77.74	76.76	80.96	69.38	61.67	54.58	61.88	85.21	71.62	66.98	74.60	68.24	72.48
	Focals Conv-F [36]	CVPR2022	92.26	85.32	82.95	86.84	-	-	-	-	-	-	-	-	-	-
	EPNet++ [38]	TPAMI2022	92.51	83.17	82.27	85.98	73.77	65.42	59.13	66.11	86.23	63.82	60.02	70.02	68.07	74.04
	DVF [33]	WACV2023	92.34	85.25	82.97	86.85	66.08	59.18	54.68	59.98	90.93	72.46	68.05	77.15	68.56	74.66
	PointPillars+ours	-	88.95	77.85	75.22	80.67	68.18	62.75	57.79	62.91	93.27	71.60	67.34	77.41	70.16	73.66
	Voxel R-CNN+ours	-	88.89	80.71	78.47	82.69	71.07	65.53	60.16	65.59	89.57	73.09	68.59	77.08	71.34	75.12

As mentioned above, the voxel size is defined as (l, w, h) . We further define a set of voxel scales $S = \{s \mid s \in [1, N_s]\}$. The voxel size in scale s is $(l * s, w * s, h * s)$.

When $s = 1$, smaller voxels lead to a higher resolution of the BEV feature map, which can keep more detailed characteristics of small objects. But it is hard to obtain enough local geometric information. Fewer points in a voxel, e.g., less than five, lead to a simple local spatial structure, suppressing the representation ability of the voxel feature. Moreover, the area of the generated VR is also small, causing many foreground pixels not gathered.

When $s > 1$, the voxels are enlarged to gather better local features, especially geometric information, benefiting from larger receptive fields. The proposed VRFM projects larger 3D space occupied by the local point cloud to get VRs, which are enlarged, too. The distribution of point clouds is sparse. With a larger voxel size, pixels in the gap between points are captured by a larger 2D region on the image plane, i.e., the image feature extracted by VRFM for each voxel includes more contextual information.

The fusion features in the scale s extracted by VRFM are defined as $\mathbf{F}_s \in \mathbb{R}^{N \times C}$. We concatenate fusion features in all scales point-wise as:

$$\mathbf{F}_S = \text{concat} \{ \mathbf{F}_s \mid s \in [1, N_s] \} \quad (7)$$

where the fusion feature \mathbf{F}_S incorporates the basic point feature, the voxel feature encoded by the PointNet-based encoder, and the image region feature extracted from the projected 2D regions in various scales. To detect objects in BEV, we use a PointNet layer to convert the sparse point-wise fusion features to voxel-level features $\mathbf{F}_{SV} \in \mathbb{R}^{V \times C}$. Then we scatter them to BEV space and use prevalent BEV backbone and 3D object detection heads for the final prediction. The proposed Multi-scale Voxelization Fusion Framework can be applied to any voxel-based LiDAR backbone.

IV. EXPERIMENTS

A. Dataset and Evaluation Metrics

We evaluate our method on the KITTI 3D and BEV object detection benchmark [39], which includes 7,481 training sam-

TABLE II
IMPROVEMENTS ON THE KITTI VAL SET USING $AP|_{R40}$ METRIC FOR PEDESTRIAN AND CYCLIST. *DENOTES RE-PRODUCED RESULTS.

Methods	3D(%)			BEV(%)		
	Pedestrian	Cyclist	mAP	Pedestrian	Cyclist	mAP
PointPillars*	52.18	67.35	59.77	58.03	71.66	64.85
PointPillars+ours	62.91	77.41	70.16	70.06	79.93	75.00
Improvement	+10.73	+10.05	+10.39	+12.02	+8.28	+10.15
Voxel R-CNN*	62.49	76.69	69.59	66.82	78.25	72.54
Voxel R-CNN+ours	65.59	77.08	71.34	69.12	79.75	74.44
Improvement	+3.10	+0.39	+1.75	+2.30	+1.50	+1.90

ples and 7,518 testing samples. Following [40], the training samples are split into 3,712 and 3,769 samples for train and val set, respectively. The samples are stratified into easy, moderate, and hard difficulties according to bounding box height, occlusion, and truncation. We calculate the mAP on the val set using 40 recall positions $AP|_{R40}$. The IoU thresholds are set to 0.7, 0.5, and 0.5 for Car, Pedestrian, and Cyclist.

We use segmentation annotations [41] for all 7481 training images to train the image backbone. The annotations include manually annotated vehicle and Pedestrian instances. We convert them to instance-agnostic annotations for semantic segmentation and use 2D bounding boxes to generate masks for Cyclists. The training samples are split for train and val set consistent with the KITTI dataset.

B. Implementation Details

Model setup. We implement our network based on two LiDAR-only baselines, PointPillars [31] and Voxel R-CNN [32]. We re-implement them by the open-sourced OpenPCDet [42] with dynamic voxelization operation [35] for a fair comparison. For PointPillars, we set the range of point cloud to $[(0, 69.12), (-39.68, 39.68), (-3, 1)]$ meters, and the base voxel size to $[0.08, 0.08, 4]$ meters along the (x, y, z) axis. For Voxel R-CNN, we set them to $[(0, 70.4), (-40, 40), (-3, 1)]$ and $[0.05, 0.05, 0.1]$, respectively. For multi-scale experiments, we set the voxel scales as $S = \{1, 4, 8\}$. We follow the approaches mentioned in [31] for LiDAR point clouds data augmentation and MoCa [43] for cross-modal data augmentation. We use

TABLE III
BEV DETECTION RESULTS ON THE KITTI VAL SET USING $AP|_{R40}$ METRIC FOR MULTI-CLASS. *DENOTES RE-PRODUCED RESULTS.

Methods	Car(%)				Pedestrian(%)				Cyclist(%)				mAP(%)
	Easy	Mod.	Hard	mAP	Easy	Mod.	Hard	mAP	Easy	Mod.	Hard	mAP	
PV-RCNN*	93.02	90.30	88.52	90.61	66.99	58.85	54.57	60.14	93.45	73.50	70.15	79.03	76.59
PointPillars*	90.86	87.31	86.28	88.15	63.06	57.57	53.47	58.03	84.51	67.43	63.03	71.66	72.61
PointPillars+ours	93.15	86.89	84.63	88.22	75.26	69.69	65.22	70.06	95.02	74.56	70.22	79.93	79.41
<i>Improvement</i>	+2.29	-0.42	-1.65	+0.07	+12.20	+12.12	+11.76	+12.02	+10.52	+7.13	+7.19	+8.28	+6.79
Voxel R-CNN*	90.89	87.05	86.91	88.29	72.37	66.52	61.57	66.82	91.23	73.28	70.25	78.25	77.79
Voxel R-CNN+ours	91.54	86.66	86.49	88.23	74.53	68.95	63.89	69.12	92.76	74.88	71.61	79.75	79.03
<i>Improvement</i>	+0.65	-0.39	-0.42	-0.05	+2.15	+2.43	+2.32	+2.30	+1.53	+1.61	+1.36	+1.50	+1.25

TABLE IV
EFFECTS OF DIFFERENT COMPONENTS ON THE KITTI VAL SET USING 3D $AP|_{R40}$ METRIC. BEST IN BOLD.

Baseline	VRFM	Multi-scale	Car(%)	Pedestrian(%)	Cyclist(%)	mAP(%)
PointPillars	✓		80.12	52.18	67.35	66.55
		✓	81.34	60.65	76.93	72.97
		✓	79.68	60.42	74.83	71.64
		✓	80.67	62.91	77.41	73.66
Voxel R-CNN	✓		83.19	62.49	76.69	74.12
		✓	82.91	64.41	75.79	74.37
		✓	83.30	62.42	76.96	74.23
		✓	82.69	65.59	77.08	75.12

TABLE V
COMPARISON BETWEEN VRFM AND PAINTING FUSION METHOD ON THE KITTI VAL SET USING 3D $AP|_{R40}$ METRIC. BEST IN BOLD.

Baseline	paint	DVFM	Car(%)	Pedestrian(%)	Cyclist(%)	mAP(%)
PointPillars	✓		79.87	63.25	76.50	73.21
		✓	80.67	62.91	77.41	73.66
Voxel R-CNN	✓		83.26	63.72	76.66	74.55
		✓	82.69	65.59	77.08	75.12

a lightweight network, LR-ASPP [44], as the image semantic segmentation backbone, and the output channel is set to 4.

Training and inference. We train the network on 2 GTX 3080 GPUs. The optimization strategy is consistent with PointPillars [31] and Voxel R-CNN [32]. During training, the LR-ASPP image backbone is frozen. We train a single model for detecting multi-class objects together and evaluate it without ensembling or testing augmentation.

C. Comparison with State-of-the-Arts

3D Results on the KITTI val set. Table I shows the 3D detection results on the val set compared with LiDAR-only and multi-modal 3D detectors. We train a single model for three classes, and our main results outperform the state-of-the-art fusion methods. Notably, our method simultaneously improves the detection accuracy of the two classes of small targets, i.e., Pedestrian and Cyclist. Our method achieves 71.34% mAP on these two classes, outperforming the state-of-the-art multi-modal method DVF [33] by 2.78%. Many samples of these classes are particularly small or truncated. Thus the LiDAR points are extremely sparse, and a small degree of misalignment can cause much noise. The results reveal that our method can effectively utilize the contextual information

from images to locate these small objects while reducing noise. Moreover, as shown in Table II, our method increases 10.39% and 1.75% mAP on PointPillars [31] and Voxel R-CNN [32] baseline for small objects, respectively. Our method shows consistent improvement for both single-stage and two-stage detection baselines.

BEV Results on the KITTI val set. BEV representation is suitable for the perception of the surrounding environment of cars benefited by near lack of occlusion. As shown in Table III, our method improves the accuracy of small objects in BEV for a large margin. As shown in Table II, our method significantly boosts the BEV mAP for both Pedestrian and Cyclist. The result on the single-stage baseline, i.e., PointPillars, achieves 75.00% mAP, surpassing the result on the two-stage Voxel R-CNN, which is 74.44%, by 0.56%. The PointPillars network scatters the pillar features directly into BEV space without height compression. This demonstrates the effectiveness of the enhanced fusion features generated by our multi-scale fusion framework.

D. Ablation Study

We perform ablation studies to verify the effect of the proposed VRFM and the multi-scale fusion framework on the KITTI val set.

Effect of each component. The baselines use hard voxelization to process the point clouds. As shown in Table IV, we reimplement the two baselines and conduct all the experiments with dynamic voxelization [35]. The multi-scale component for the LiDAR-only network is reimplemented following HVNet [22], and the mean voxel feature encoder of Voxel R-CNN is replaced. For PointPillars, which has a simple voxel feature encoder, the multi-scale component or the VRFM with single-scale both improves the performance for a large margin. This may be due to the fact that the extracted information enriches the feature of a single pillar. Still, combing with the proposed VRFM, the multi-scale fusion framework brings performance gain of 2.49% and 2.58% mAP over the single-modal results for Pedestrian and Cyclist, respectively. Image features from nearby areas at multiple scales are fused with voxel features generated by multi-scale voxelization operation. As for the Voxel R-CNN baseline, the VRFM component with single-scale reduces performance on Car and Cyclist. However, the multi-scale fusion framework with multi-modal input

still improves the results on small objects and the multi-class mAP. It achieves a relative gain of 3.10% and 0.39% mAP for Pedestrian and Cyclist over the baseline, respectively. This strongly demonstrates the effectiveness of the proposed Multi-scale Voxelization Fusion Framework. With appropriate multi-modal and multi-scale contextual information, the network is able to locate small objects effectively.

Comparison with sparse fusion. The common fusion strategy of establishing one-to-one mappings between LiDAR points and image pixels is too sparse for appropriate fusion. In Table V, we compare the painting fusion methods and our region voxel fusion methods. The painting networks are modified from the proposed multi-scale fusion framework for a fair comparison. The painting operation is implemented following [6] by sampling pixels for every projected point to replace the VRFM. The other parts of the network and the training schedule remain the same. As shown in Table V, the mAP of the proposed network with VRFM outperforms the painting fusion method on both two baselines. For small-size classes on the Voxel R-CNN baseline, our method surpasses the painting method by a large margin. This strongly demonstrates that the dense correspondence and contextual information obtained by our fusion strategy can relieve the sparsity problem caused by small size and far distance.

V. CONCLUSION

In this paper, we propose the Region Voxel Fusion Module to achieve a dense and effective fusion between sparse LiDAR points and dense image pixels. The contextual information from both modalities is integrated to enrich the voxel features, and the background noise is reduced, benefiting from better alignment. Moreover, we propose a Multi-scale Voxelization Fusion Framework to fuse local point clouds with image regions in various scales and deal with the problem of varying scales of target objects. Extensive experiments on the KITTI dataset show that the proposed SDVRF is able to achieve better performance on multi-class 3D and BEV detection, especially for small objects like Pedestrian and Cyclist. Our method is able to be applied to other LiDAR-based methods, and we hope our method can serve as a better alternative to the current fusion strategies for multi-modal 3D objection.

ACKNOWLEDGMENT

This work was supported partly by the National Natural Science Foundation of China (Grant No. 62173045, 61673192), partly by the Fundamental Research Funds for the Central Universities (Grant No. 2020XD-A04-3), and the Natural Science Foundation of Hainan Province (Grant No. 622RC675).

REFERENCES

- [1] Jiageng Mao, Shaoshuai Shi, Xiaogang Wang, and Hongsheng Li. 3d object detection for autonomous driving: a review and new outlooks. *arXiv preprint arXiv:2206.09474*, 2022.
- [2] Rui Qian, Xin Lai, and Xirong Li. 3d object detection for autonomous driving: a survey. *Pattern Recognition*, 130:108796, 2022.
- [3] Yingjie Wang, Qiuyu Mao, Hanqi Zhu, Jiajun Deng, Yu Zhang, Jianmin Ji, Houqiang Li, and Yanyong Zhang. Multi-modal 3d object detection in autonomous driving: a survey. *arXiv preprint arXiv:2106.12735*, 2021.
- [4] Vishwanath A Sindagi, Yin Zhou, and Oncel Tuzel. Mvx-net: Multimodal voxelnet for 3d object detection. In *2019 International Conference on Robotics and Automation (ICRA)*, pages 7276–7282. IEEE, 2019.
- [5] Tengpeng Huang, Zhe Liu, Xiwu Chen, and Xiang Bai. Epnet: Enhancing point features with image semantics for 3d object detection. In *Computer Vision—ECCV 2020: 16th European Conference, Glasgow, UK, August 23–28, 2020, Proceedings, Part XV 16*, pages 35–52. Springer, 2020.
- [6] Sourabh Vora, Alex H Lang, Bassam Helou, and Oscar Beijbom. Pointpainting: Sequential fusion for 3d object detection. In *Proceedings of the IEEE/CVF conference on computer vision and pattern recognition*, pages 4604–4612, 2020.
- [7] Liang Xie, Chao Xiang, Zhengxu Yu, Guodong Xu, Zheng Yang, Deng Cai, and Xiaofei He. Pi-rcnn: An efficient multi-sensor 3d object detector with point-based attentive cont-conv fusion module. In *Proceedings of the AAAI conference on artificial intelligence*, pages 12460–12467, 2020.
- [8] Chunwei Wang, Chao Ma, Ming Zhu, and Xiaokang Yang. Pointaugmenting: Cross-modal augmentation for 3d object detection. In *Proceedings of the IEEE/CVF Conference on Computer Vision and Pattern Recognition*, pages 11794–11803, 2021.
- [9] Yingwei Li, Adams Wei Yu, Tianjian Meng, Ben Caine, Jiquan Ngiam, Daiyi Peng, Junyang Shen, Yifeng Lu, Denny Zhou, Quoc V Le, et al. Deepfusion: Lidar-camera deep fusion for multi-modal 3d object detection. In *Proceedings of the IEEE/CVF Conference on Computer Vision and Pattern Recognition*, pages 17182–17191, 2022.
- [10] Xiaopei Wu, Liang Peng, Honghui Yang, Liang Xie, Chenxi Huang, Chengqi Deng, Haifeng Liu, and Deng Cai. Sparse fuse dense: Towards high quality 3d detection with depth completion. In *Proceedings of the IEEE/CVF Conference on Computer Vision and Pattern Recognition*, pages 5418–5427, 2022.
- [11] Wenqi Zheng, Han Xie, Yunfan Chen, Jeongjin Roh, and Hyunchul Shin. Pifnet: 3d object detection using joint image and point cloud features for autonomous driving. *Applied Sciences*, 12(7):3686, 2022.
- [12] Charles R Qi, Hao Su, Kaichun Mo, and Leonidas J Guibas. Pointnet: Deep learning on point sets for 3d classification and segmentation. In *Proceedings of the IEEE conference on computer vision and pattern recognition*, pages 652–660, 2017.
- [13] Xiaozhi Chen, Huimin Ma, Ji Wan, Bo Li, and Tian Xia. Multi-view 3d object detection network for autonomous driving. In *Proceedings of the IEEE conference on Computer Vision and Pattern Recognition*, pages 1907–

- 1915, 2017.
- [14] Zhixin Wang and Kui Jia. Frustum convnet: Sliding frustums to aggregate local point-wise features for amodal 3d object detection. In *2019 IEEE/RSJ International Conference on Intelligent Robots and Systems (IROS)*, pages 1742–1749. IEEE, 2019.
- [15] Ming Liang, Bin Yang, Yun Chen, Rui Hu, and Raquel Urtasun. Multi-task multi-sensor fusion for 3d object detection. In *Proceedings of the IEEE/CVF Conference on Computer Vision and Pattern Recognition*, pages 7345–7353, 2019.
- [16] Jin Hyeok Yoo, Yecheol Kim, Jisong Kim, and Jun Won Choi. 3d-cvf: Generating joint camera and lidar features using cross-view spatial feature fusion for 3d object detection. In *Computer Vision–ECCV 2020: 16th European Conference, Glasgow, UK, August 23–28, 2020, Proceedings, Part XXVII 16*, pages 720–736, 2020.
- [17] Ming Liang, Bin Yang, Shenlong Wang, and Raquel Urtasun. Deep continuous fusion for multi-sensor 3d object detection. In *Proceedings of the European conference on computer vision (ECCV)*, pages 641–656, 2018.
- [18] Pei An, Junxiong Liang, Kun Yu, Bin Fang, and Jie Ma. Deep structural information fusion for 3d object detection on lidar–camera system. *Computer Vision and Image Understanding*, 214:103295, 2022.
- [19] Xin Li, Botian Shi, Yuenan Hou, Xingjiao Wu, Tianlong Ma, Yikang Li, and Liang He. Homogeneous multi-modal feature fusion and interaction for 3d object detection. In *Computer Vision–ECCV 2022: 17th European Conference, Tel Aviv, Israel, October 23–27, 2022, Proceedings, Part XXXVIII*, pages 691–707. Springer, 2022.
- [20] Chunmian Lin, Daxin Tian, Xuting Duan, Jianshan Zhou, Dezong Zhao, and Dongpu Cao. 3d-dfm: anchor-free multimodal 3-d object detection with dynamic fusion module for autonomous driving. *IEEE Transactions on Neural Networks and Learning Systems*, 2022.
- [21] Yin Zhou, Pei Sun, Yu Zhang, Dragomir Anguelov, Jiyang Gao, Tom Ouyang, James Guo, Jiquan Ngiam, and Vijay Vasudevan. End-to-end multi-view fusion for 3d object detection in lidar point clouds. In *Conference on Robot Learning*, pages 923–932. PMLR, 2020.
- [22] Maosheng Ye, Shuangjie Xu, and Tongyi Cao. Hynet: Hybrid voxel network for lidar based 3d object detection. In *Proceedings of the IEEE/CVF conference on computer vision and pattern recognition*, pages 1631–1640, 2020.
- [23] Bin Yang, Wenjie Luo, and Raquel Urtasun. Pixor: Real-time 3d object detection from point clouds. In *Proceedings of the IEEE conference on Computer Vision and Pattern Recognition*, pages 7652–7660, 2018.
- [24] Zetong Yang, Yanan Sun, Shu Liu, Xiaoyong Shen, and Jiaya Jia. Ipod: Intensive point-based object detector for point cloud. *arXiv preprint arXiv:1812.05276*, 2018.
- [25] Shaoshuai Shi, Xiaogang Wang, and Hongsheng Li. Pointcnn: 3d object proposal generation and detection from point cloud. In *Proceedings of the IEEE/CVF conference on computer vision and pattern recognition*, pages 770–779, 2019.
- [26] Shaoshuai Shi, Chaoxu Guo, Li Jiang, Zhe Wang, Jianping Shi, Xiaogang Wang, and Hongsheng Li. Pv-rcnn: Point-voxel feature set abstraction for 3d object detection. In *Proceedings of the IEEE/CVF Conference on Computer Vision and Pattern Recognition*, pages 10529–10538, 2020.
- [27] Weijing Shi and Raj Rajkumar. Point-gnn: Graph neural network for 3d object detection in a point cloud. In *Proceedings of the IEEE/CVF conference on computer vision and pattern recognition*, pages 1711–1719, 2020.
- [28] Zetong Yang, Yanan Sun, Shu Liu, and Jiaya Jia. 3dssd: Point-based 3d single stage object detector. In *Proceedings of the IEEE/CVF conference on computer vision and pattern recognition*, pages 11040–11048, 2020.
- [29] Wu Zheng, Weiliang Tang, Li Jiang, and Chi-Wing Fu. Se-ssd: Self-ensembling single-stage object detector from point cloud. In *Proceedings of the IEEE/CVF Conference on Computer Vision and Pattern Recognition*, pages 14494–14503, 2021.
- [30] Yifan Zhang, Qingyong Hu, Guoquan Xu, Yanxin Ma, Jianwei Wan, and Yulan Guo. Not all points are equal: Learning highly efficient point-based detectors for 3d lidar point clouds. In *Proceedings of the IEEE/CVF Conference on Computer Vision and Pattern Recognition*, pages 18953–18962, 2022.
- [31] Alex H Lang, Sourabh Vora, Holger Caesar, Lubing Zhou, Jiong Yang, and Oscar Beijbom. Pointpillars: Fast encoders for object detection from point clouds. In *Proceedings of the IEEE/CVF conference on computer vision and pattern recognition*, pages 12697–12705, 2019.
- [32] Jiajun Deng, Shaoshuai Shi, Peiwei Li, Wengang Zhou, Yanyong Zhang, and Houqiang Li. Voxel r-cnn: Towards high performance voxel-based 3d object detection. In *Proceedings of the AAAI Conference on Artificial Intelligence*, pages 1201–1209, 2021.
- [33] Anas Mahmoud, Jordan SK Hu, and Steven L Waslander. Dense voxel fusion for 3d object detection. In *Proceedings of the IEEE/CVF Winter Conference on Applications of Computer Vision*, pages 663–672, 2023.
- [34] Andrew Howard, Mark Sandler, Grace Chu, Liang-Chieh Chen, Bo Chen, Mingxing Tan, Weijun Wang, Yukun Zhu, Ruoming Pang, Vijay Vasudevan, et al. Searching for mobilenetv3. In *Proceedings of the IEEE/CVF international conference on computer vision*, pages 1314–1324, 2019.
- [35] Yin Zhou, Pei Sun, Yu Zhang, Dragomir Anguelov, Jiyang Gao, Tom Ouyang, James Guo, Jiquan Ngiam, and Vijay Vasudevan. End-to-end multi-view fusion for 3d object detection in lidar point clouds. In *Conference on Robot Learning*, pages 923–932, 2020.
- [36] Yukang Chen, Yanwei Li, Xiangyu Zhang, Jian Sun, and Jiaya Jia. Focal sparse convolutional networks for 3d object detection. In *Proceedings of the IEEE/CVF Conference on Computer Vision and Pattern Recognition*, pages 5428–5437, 2022.

- [37] Jordan SK Hu, Tianshu Kuai, and Steven L Waslander. Point density-aware voxels for lidar 3d object detection. In *Proceedings of the IEEE/CVF Conference on Computer Vision and Pattern Recognition*, pages 8469–8478, 2022.
- [38] Zhe Liu, Tengting Huang, Bingling Li, Xiwu Chen, Xi Wang, and Xiang Bai. EpNet++: Cascade bi-directional fusion for multi-modal 3d object detection. *IEEE Transactions on Pattern Analysis and Machine Intelligence*, 2022.
- [39] Andreas Geiger, Philip Lenz, and Raquel Urtasun. Are we ready for autonomous driving? the kitti vision benchmark suite. In *2012 IEEE conference on computer vision and pattern recognition*, pages 3354–3361. IEEE, 2012.
- [40] Xiaozhi Chen, Kaustav Kundu, Yukun Zhu, Andrew G Berneshawi, Huimin Ma, Sanja Fidler, and Raquel Urtasun. 3d object proposals for accurate object class detection. *Advances in neural information processing systems*, 28, 2015.
- [41] Jonas Heylen, Mark De Wolf, Bruno Dawagne, Marc Proesmans, Luc Van Gool, Wim Abbeloos, Hazem Abdelkawy, and Daniel Olmeda Reino. Monocinis: Camera independent monocular 3d object detection using instance segmentation. In *Proceedings of the IEEE/CVF International Conference on Computer Vision*, pages 923–934, 2021.
- [42] OpenPCDet Development Team. Openpcdet: An open-source toolbox for 3d object detection from point clouds. <https://github.com/open-mmlab/OpenPCDet>, 2020.
- [43] Wenwei Zhang, Zhe Wang, and Chen Change Loy. Exploring data augmentation for multi-modality 3d object detection. *arXiv preprint arXiv:2012.12741*, 2020.
- [44] Andrew Howard, Mark Sandler, Grace Chu, Liang-Chieh Chen, Bo Chen, Mingxing Tan, Weijun Wang, Yukun Zhu, Ruoming Pang, Vijay Vasudevan, et al. Searching for mobilenetv3. In *Proceedings of the IEEE/CVF international conference on computer vision*, pages 1314–1324, 2019.